

Calculating Earth Impedances For Underground Transmission Cables

F. A. Uribe

J. L. Naredo

P. Moreno

L. Guardado

CINVESTAV, Unidad Guadalajara.
 ProL. López Mateos Sur 590, CP.45090
 Guadalajara, Jalisco, México.
fauribe@gdl.cinvestav.mx

Instituto Tecnológico
 de Morelia, México.

Abstract – An analysis of Pollaczek’s integral is presented in this paper. It reveals the difficulties found when attempting its numerical solution. The analysis provided here further indicates a strategy to avoid these difficulties. A numerical algorithm is then described and implemented. Solutions to Pollaczek’s integral are provided in graphical form for a broad range of applications. Finally, the graphical results are used to establish validity ranges of two well known approximations of Pollaczek’s integral.

Keywords: Underground Transmission, Pollaczek’s Integral, Earth Return Impedance, Cable Parameters.

I. INTRODUCTION

The existing methods to perform electromagnetic analysis of aerial lines can be considered well established. For underground transmission systems, however, the currently available methods still require further development. This is due in part to the large variety of cable geometries being used. Another difficulty is the analysis of electromagnetic fields inside an imperfect conducting ground. To calculate buried cable ground impedances one has to solve Pollaczek’s integral [1] which, as the one by Carson, does not have an analytical solution [2]. Carson’s integral, however, can be solved numerically with relative ease and counts in addition with satisfactory approximations [3,4].

Pollaczek’s integrand is highly oscillatory and irregular. For this reason its integration by series or by general algorithms presents convergence problems [2,5,7]. Wedepohl and Wilcox have proposed a series solution to Pollaczek’s integral [5]. This series is very cumbersome and has convergence difficulties at certain application ranges [2,5].

In this paper an analysis of Pollaczek’s integrand is first presented. On the basis of this analysis, a numerical integration algorithm is then developed. The resulting algorithm is very reliable and highly efficient from the computational stand point. Solutions to Pollaczek’s integral are further provided in graphical form for most cases of practical interest. Finally, these solutions are applied in the evaluation of two very common approximations provided in [2] and [6].

II. POLLACZEK’S INTEGRAL

Fig. 1 shows a system of two underground cables. Its self and mutual ground impedances are calculated through the following formulas [1,2]:

$$Z_t = \frac{j\omega\mu_0}{2\pi} [K_0(d/p) - K_0(D/p) + J] \quad (1a)$$

and

$$J = \int_{-\infty}^{+\infty} \frac{\exp\left[-2h\sqrt{\beta^2 + 1/(p)^2}\right]}{|\beta| + \sqrt{\beta^2 + 1/(p)^2}} \exp(j\beta x) d\beta, \quad (1b)$$

where:

- ω — angular frequency,
- μ_0 — magnetic permeability of air and soil,
- σ — soil conductivity,
- $K_0()$ — modified Bessel function of second class and zero order,
- d — distance between cables (for the self impedance this is the cable radius),
- D — distance between one cable and the image of the other (for the self impedance this is two times the cable depth),
- p — complex depth of the Skin Effect layer
 $p = 1/\sqrt{j\omega\mu_0\sigma}$,
- h — depth of cable (for the mutual impedance this is the average depth
 $h = (h_1 + h_2)/2$)
- and
- x — horizontal distance between cables (for self impedance this is the cable radius).

Expression (1b) corresponds to Pollaczek’s integral as obtained when the ground has magnetic permeability equal to μ_0 . This assumption which, for the sake of clarity, has been adopted here can be removed through the considerations provided in this paper’s appendix.

Integral (1b) is transformed into a more convenient form as follows. The following change of variable is introduced first:

$$\beta = \sqrt{\alpha} u \quad (2a)$$

where

$$\sqrt{\alpha} = 1/|p| = \sqrt{\omega\mu_0\sigma} \quad (2b)$$

With this change and after some mathematical manipulations (1b) becomes:

$$J = 2 \int_0^{+\infty} \frac{\exp\left[-2h\sqrt{\alpha}\sqrt{u^2 + j}\right]}{u + \sqrt{u^2 + j}} \cos(\sqrt{\alpha} x u) du. \quad (3)$$

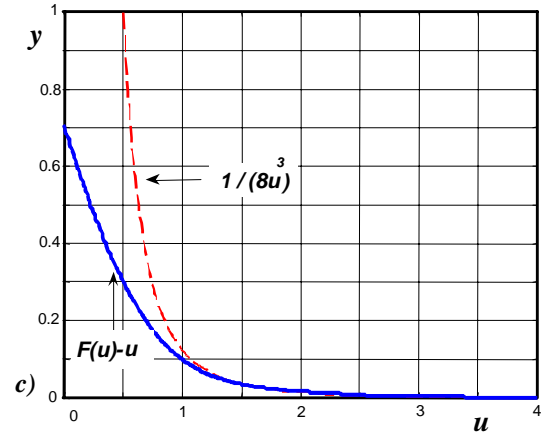
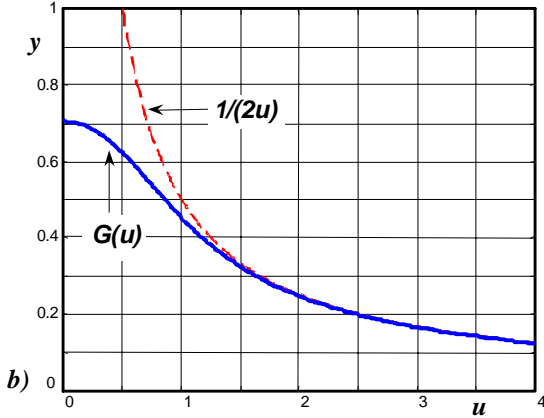
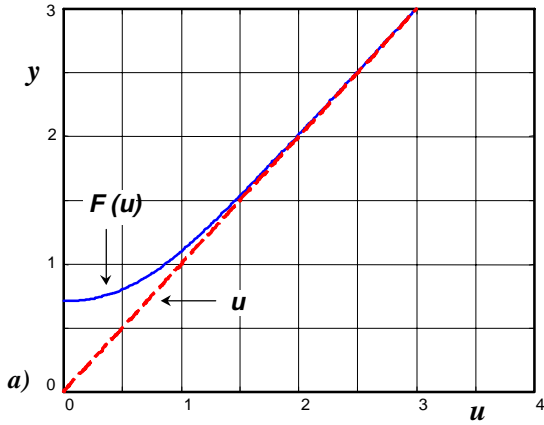


Fig 2.- Plots of functions of u and of their asymptotic approximations. **a)** $y = F(u)$, **b)** $y = G(u)$ and **c)** $y = F(u) - u$.

Expression (14c) is adopted here as the truncation criterion for the numerical solution of Pollaczek's integral. The value of $\lambda=6.0$ has been established empirically here as satisfactory, for as long as $u_{max} \geq 2$; otherwise, $u_{max}=2$ and, from (14c), $\lambda=2\xi$.

The third factor in (9) is readily identified as a complex term with irregular oscillations. On expanding it as follows:

$$\exp[-j \cdot \xi G(u)] = \cos[\xi G(u)] - j \cdot \sin[\xi G(u)], \quad (15a)$$

it becomes clear that this term does not oscillate if:

$$\xi G(u) < \pi/2; \quad (15b)$$

or, since the maximum value of $G(u)$ is $G(0)=\sqrt{2}/2$, expression (15a) will oscillate for:

$$\xi > \pi\sqrt{2}/2 = 2.22144 \quad (15c)$$

Fig. 3 illustrates a plot of $\xi \cdot G(u)$ for a value of ξ greater than 2.22144. Each value of $\xi \cdot G(u)$ which is an odd multiple of $\pi/2$ corresponds to a zero crossing of the cosine term in (15a). Even multiples of $\pi/2$ are the zeros for the sine term. The total number of zeros is:

$$n_i = \inf\left\{\sqrt{2}\xi/\pi\right\}, \quad (15d)$$

where "inf {x}" denotes the nearest integer equal or smaller to positive x. The values of u corresponding to these zeros are easily obtained as follows:

$$u_k = G^{-1}\left(\frac{k\pi}{\xi\sqrt{2}}\right) = \frac{\sqrt{\xi^4 - k^4\pi^4/4}}{\xi k\pi}, \quad k = n_i, \dots, 2, 1 \quad (15f)$$

Fig. 4a provides a set of plots for $\cos[\xi G(u)]$ at different values of ξ , while Fig. 4b shows the corresponding plots for $\sin[\xi G(u)]$. The irregular and oscillatory behavior of this third factor of (9) is apparent in these two figures.

The fourth factor of (9) is the cosine function of $\xi\eta u$. This thus is an oscillatory regular term. The number of zeros of this factor within the truncated interval of u "[0, u_{max}]" is:

$$z_2 = \inf\left\{\frac{\xi\eta u_{max}}{\pi} + \frac{1}{2}\right\} \quad (16)$$

According to (14c) and (16) the fourth factor does not present oscillations between 0.0 and u_{max} if

$$\eta < \pi / (2\xi u_{max}). \quad (17)$$

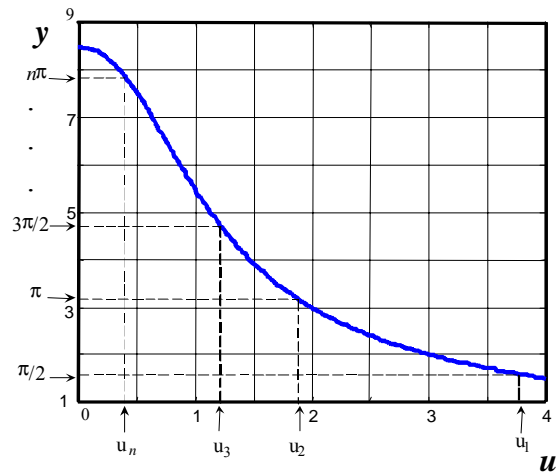


Fig. 3.- Plot of $y = 12 \cdot G(u)$.

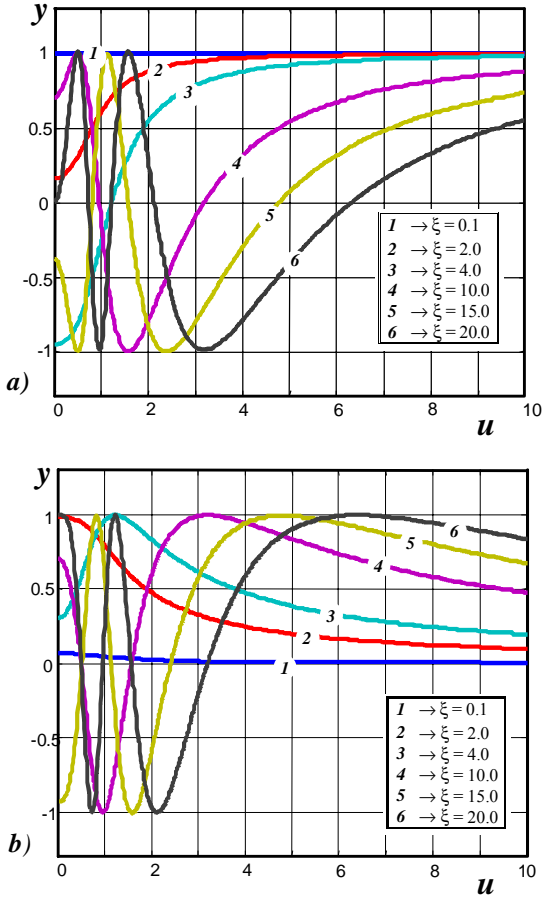


Fig. 4.- a) Plot of $y = \cos[-\xi G(u)]$ for various values of ξ . b) Plot of $y = \sin[\xi G(u)]$ for values of ξ .

IV. NUMERICAL SOLUTION OF POLLACZEK'S INTEGRAL

The previous analysis reveals that a major source of difficulties when solving numerically Pollaczek's integral is the highly irregular oscillation pattern of its integrand. This pattern is caused by the combination of the third and the fourth factors of (9) and it makes practically impossible to establish rules regarding the number and widths of the oscillation lobes.

The above analysis leads also to the following numerical procedure that circumvents the previously mentioned difficulties. First, u_{\max} is determined from (14c) and from an empirically predetermined λ . The numerical integration range is thus established as $[0, u_{\max}]$. Then, all the values of u that are inside $[0, u_{\max}]$ and that correspond to a zero of one of the following functions are determined and ordered into a vector $\mathbf{U}=(u_1, u_2, \dots, u_n)$:

$$\cos [\xi G(u)], \quad (18)$$

$$\sin [\xi G(u)] \quad (19)$$

and

$$\cos [\eta \xi u]. \quad (20)$$

Note that (18) and (19) are the real and imaginary parts of (15a), respectively, and that (20) is the fourth factor in (9). The width of the integrand's first lobe is u_1 ; *i. e.*, the first component of \mathbf{U} . The width of the last lobe is $u_{\max}-u_n$.

Next, the truncated integration range $[0, u_{\max}]$ is divided into the following $n+1$ subranges:

$$[0, u_1], \quad [u_1, u_2], \quad \dots \quad [u_n, u_{\max}]$$

Due to the form in which these subranges are established, each oscillation lobe of the real and imaginary parts of the integrand will encompass only one or two complete contiguous subranges. Next, each one of the subranges is further divided in N equally spaced values of u . The evaluation of the integrand of (9) in the resulting $N \times (n+1)$ values of u guarantees that each lobe is represented by at least N samples. Finally, the application of a simple quadrature method (Trapezoidal, Simpson, etc) to all these samples yields a numerical solution of Pollaczek's integral which converges uniformly as $N \rightarrow \infty$.

Parameters ξ and η depend on the physical variables h , ω , σ and x . It is considered here that for most practical situations these variables are within the following ranges:

$$\begin{aligned} 0.2 &\leq h \leq 10 && [\text{m}] \\ 2\pi &\leq \omega \leq 2\pi \times 10^6 && [\text{rad/s}] \\ 10^{-4} &\leq \sigma \leq 1 && [\text{S/m}] \end{aligned}$$

and

$$0.1 \leq x \leq 100 \quad [\text{m}]$$

These ranges are contained well within the following ones for ξ and η :

$$\begin{aligned} 10^{-4} &\leq \xi \leq 20 \\ 10^{-3} &\leq \eta \leq 100 \end{aligned}$$

The previously described algorithm is now applied in the solution of Pollaczek's integral for values of ξ and η inside these ranges. Figs. 5a and 5b provide these results in graphical form. These figures were generated solving Pollaczek's integral 287 times. The time required for this task by a Pentium™ II PC at 350 MHz, running in MATLAB® V. 5.3.0, was slightly less than 1 second.

V. EVALUATING SIMPLIFIED SOLUTION METHODS

The difficulties posed by Pollaczek's integral have motivated the search for simplified solutions to it. One that is widely used in EMTP applications was proposed by Ametani [2]. It consists in approximating Pollaczek's by Carson's integral. Another important approximation has been recently proposed in [6]. This is based on Cauchy integral theorem and in the complex depth of images method [3].

The results plotted in Figs. 5a and 5b have been tested increasing the discretization level N in up to four orders of magnitude. It has been found that the changes are well below 0.1 %. These results now are applied in the evaluation of the two above mentioned simplified solutions. Fig. 6a provides curves of percent magnitude errors in Ametani's method. Fig. 6b provides similar error curves for the approximation proposed in [6]. These two sets of plots are obtained taking as reference the values from Figs. 5a and 5b.

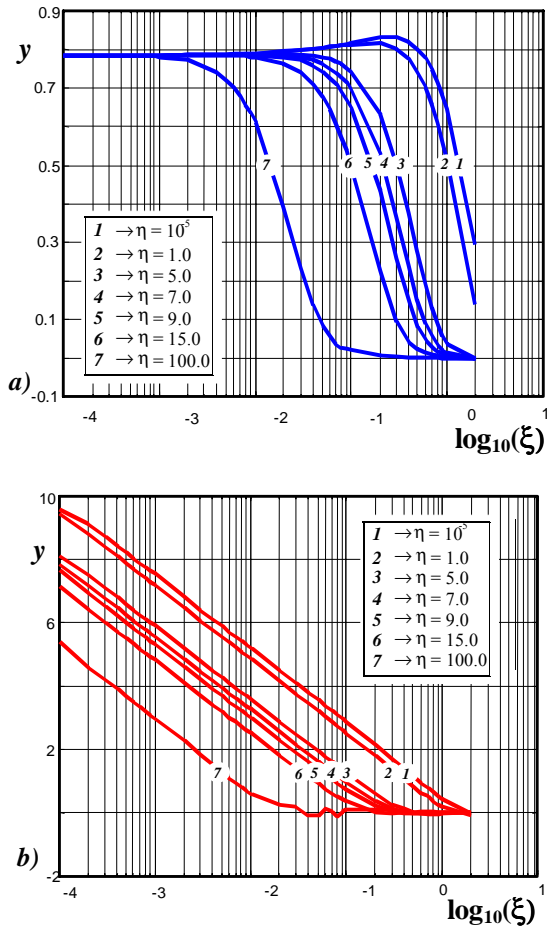


Fig. 5.- Numerical solution of (1b) divided by $-2j$ for various values of ξ and η . *a)* $\Re\{J\}$, *b)* $\Im\{J\}$.

From a comparative analysis of Figs. 6a and 6b one can observe that both simplified methods provide similar approximations for most values of ξ and η . For all the values of η considered, except $\eta = 100$, and for $10^{-4} \leq \xi \leq 10^{-1}$ both simplified methods present errors below 10%. For $\eta = 100$ Ametani's method performs much better than the one in [6].

In addition to the two previously considered simplified methods, various others that have been proposed in the specialized literature could be tested using the method proposed here. These authors consider that the latter is a complement of the former ones.

VI. CONCLUSIONS

An analysis of Pollaczek's integral has been proposed here. Through this analysis it has been possible to determine the pitfalls found at solving this integral with standard numerical algorithms. The analysis has indicated, in addition, a strategy to avoid these pitfalls. An algorithm based on this strategy has been described and implemented in MATLAB[®]. Solutions to Pollaczek's integral have been provided in graphical form for a very broad range of applications.

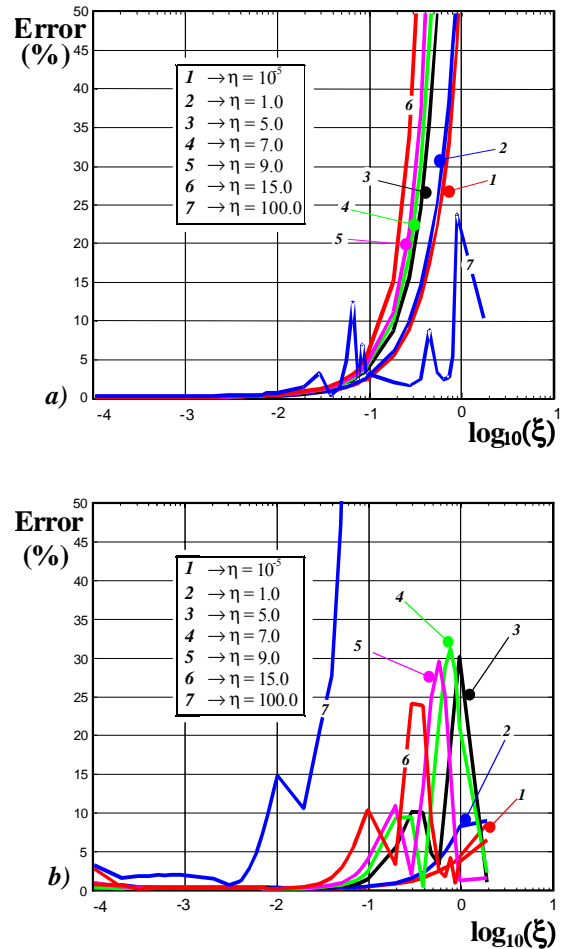


Fig. 6.- Percent errors of approximations to Pollaczek's integral. *a)* Ametani's approximation. *b)* Saad, Gaba, Giroux formula.

These solutions have been further applied at evaluating and determining applications ranges of the two approximates solutions of Pollaczek's integral previously provided by other authors. Finally, these authors consider that the algorithms derived from the analysis presented here are complementary to various other approximations to Pollaczek's integral that are available from the specialized literature.

VII. ACKNOWLEDGMENT.

The authors wish to thank the National Council of Science and Technology of Mexico (CONACYT) for the financial support provided through project no. 34698-A.

VIII. REFERENCES

- [1] F. Pollaczek, "Sur le champ produit par un conducteur simple infiniment long parcouru par un courant alternatif", *Revue Gén. Elec*, vol. 29, 1931, pp. 851-867,
- [2] H. W. Dommel, *Electromagnetic Transients Program Reference Manual (EMTP Theory Book)*, Prepared for Bonneville Power Administration, P.O. Box 3621, Portland, Ore., 97208, USA, 1986.

- [3] C. Gary, "Approche complete de la propagation multifilaire en Haute frequence par utilisation des matrices complexes", E.D.F Bulletin de la Direction des Etudes et Recherches, serie B, No. 3/4, 1976, pp.5-20.
- [4] F. Alvarado, R. Betancourt, "An accurate closed-form approximation for ground return impedance calculations", *Proceedings of the IEEE*, vol.71, No.2, February 1983, pp.279-280.
- [5] L. M. Wedepohl, D. J Wilcox, "Transient analysis of underground power-transmission systems", *Proc. IEE*, vol. 120, No. 2, February 1973, pp. 253-260.
- [6] O. Saad, G. Gaba, M. Giroux, "A closed-form approximation for ground return impedance of underground cables", *IEEE Trans. on Power Delivery*, vol.11, No.3, July 1996, pp. 1536-1545.
- [7] T. T. Nguyen, "Earth-return path impedances of underground cables. Part 1: Numerical integration of infinite integrals", *IEE Proc.-Gener. Transm. Distrib.*, vol. 145, No. 6, November 1998, pp. 621-626.

IX. APPENDIX.- EFFECTS OF EARTH PERMEABILITY

Let the ground have a relative magnetic permeability μ_r which generally is different from the $\mu_r=1$ assumed in (1b). The first factor of (9) still preserves the form $H(u) + jM(u)$, with $H(u)$ and $M(u)$ decreasing monotonic; just that now

$$\mu_r u + \sqrt{u^2 + j} \quad (A1)$$

replaces

$$u + \sqrt{u^2 + j} \quad (A2)$$

in (4).

Figs. A1 and A2 provide plots of $H(u)$ and $M(u)$, respectively, for various values of μ_r . Note from these two figures that for $\mu_r=1$:

$$H(u) = F(u) - u \quad (A3)$$

and

$$M(u) = G(u). \quad (A4)$$

Note also that $H(u)$ and $M(u)$ can still be regarded as "low pass" damping envelopes. The extension of section IV algorithm to the case $\mu_r \neq 1$ should thus be straightforward.

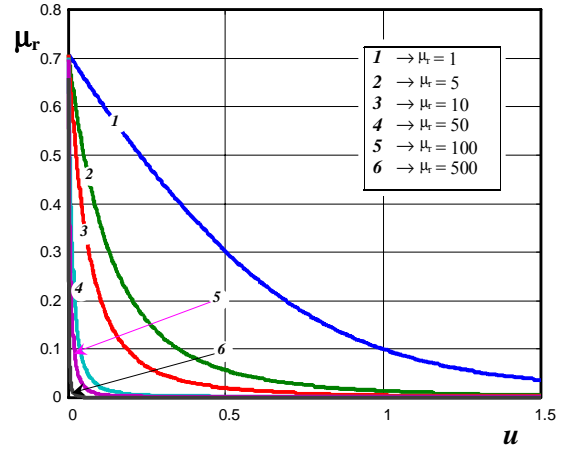


Fig. A1.- Plot of $\Re\{-2j(\mu_r \cdot u + \sqrt{u^2 + j})^{-1}\}$.

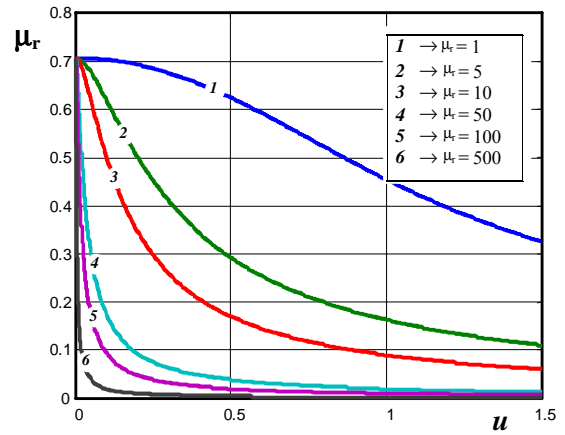


Fig. A2.- Plot of $\Im\{-2j(\mu_r \cdot u + \sqrt{u^2 + j})^{-1}\}$.